

How round is round? On accuracy in complex dielectric permittivity calculations: A finite-size scaling approach *

Enis Tuncer †

Chalmers University of Technology, SE-412 96 Gothenburg Sweden

Received October 28, 2018

Abstract

Accuracy in complex dielectric permittivity calculations in binary dielectric mixtures in two-dimensions are reported by taking into account the shape of the inclusion phase. The dielectric permittivity of the mixtures were calculated using the finite element, and the permittivities were estimated by two different procedures. The results were compared with those of analytical models based on mean field approximation and regular arrangement of disks. We have approached the problem emphasizing the finite-size behavior in which regular polygons with n sides were assumed to mimic the disk inclusion phase. It was found that at low concentrations, $< 30\%$, considering an decagon ($n = 10$) cause an error of $< 0.1\%$ in the effective medium quantities compared with the results obtained using the analytical models. **Key Words:** Dielectric mixtures, composite materials, the finite element method, finite size scaling.

1. Introduction

To predict and to better design (tailor) composite materials for electrical applications, such as composite insulators [1, 2] and electromagnetic shields [3], *etc*, have been a challenge for both theoretical and practical importance [4]. In early days of electromagnetics theory, effective electrical properties, *i.e.*, conductivity, σ , and permittivity, ϵ , of systems composed of two phases have been calculated analytically by effective mean field approaches [5, 6, 7, 8, 9] (EMA) and regular arrangement of disks [10, 11] (RAD). And nowadays, computer simulations have become as an alternative way of doing science closer

*Financed by the ELIS program of the Swedish Foundation for Scientific Research (SSF).

†email: enis.tuncer@physics.org; Currently at Department of Physics, University of Potsdam, Potsdam 14469 Germany.

to experiment than theory but complementary to both. Moreover, with the help of new computation techniques to solve partial differential equations, numerical simulations of more complex systems, such as systems with several components with arbitrary shapes, can be considered and desired properties can be calculated. However, like experiments, computer simulations produce data rather than theories and should be judged on the quality of those data. Accordingly, the reliability of the applied technique and accuracy of the obtained results must be checked and be verified either by analytical solutions or by performing the same calculations with a different technique or tool [12]. The latter procedure can be, for example, applications of the finite element and the finite difference methods to the same problem. The former one, to verify with an analytical solution, is not, on the other hand, an easy task in most of the cases, in which either there are no analytical solutions or approximations are considered in the analytical solutions. Moreover, when the numerical results are taken into consideration, there are plausible sources of errors which originate from the model. The numerical errors can be eliminated by changing the order of the applied model or the discretization method used.

In this paper, the accuracy in the numerical calculations of effective electrical properties of a binary dielectric mixture is reported by taking into account the finite-size scaling. A field simulation software, based on the finite element method (FEM), has been used, and the effective properties has been calculated by two different ways. The results were compared with those of two analytical solutions, which are based on EMA and RAD.

2. Electrical properties of binary mixtures

Electrical properties of materials can be described by the dependence of either the complex dielectric permittivity, $\varepsilon(\omega)$, or complex (AC) conductivity, $\varsigma(\omega)$, on the frequency, ω and on the external variables such as temperature, pressure, humidity *etc.* Both of these quantities can be expressed in terms of one and other. Therefore, a general complex dielectric response of materials can be describe with the complex dielectric susceptibility, $\chi(\omega)$,

$$\varepsilon(\omega) = \epsilon + \chi'(\omega) - \imath\chi''(\omega) + \frac{\sigma}{\imath\epsilon_0\omega} \quad (1)$$

$$\varsigma(\omega) = \imath\epsilon_0\omega\varepsilon(\omega) \quad (2)$$

where $\imath = \sqrt{-1}$ and ϵ_0 is the dielectric permittivity of free space, $1/36\pi$ nF/m. ϵ and σ are the dielectric constant at optical frequencies and ohmic conductivity of the material, respectively. Moreover, the simplest form of dielectric relaxation, $\chi(\omega)$, is observed for dilute solutions (mixtures) and ferroelectric materials [13], and is expressed in Debye form [14]

$$\chi(\omega) = \chi(0)[1 + \imath\omega\tau]^{-1} \quad (3)$$

where $\chi(0)$ and τ are the dielectric strength and relaxation time (inverse relaxation rate) of the polarization. At frequencies much higher and lower than inverse relaxation time,

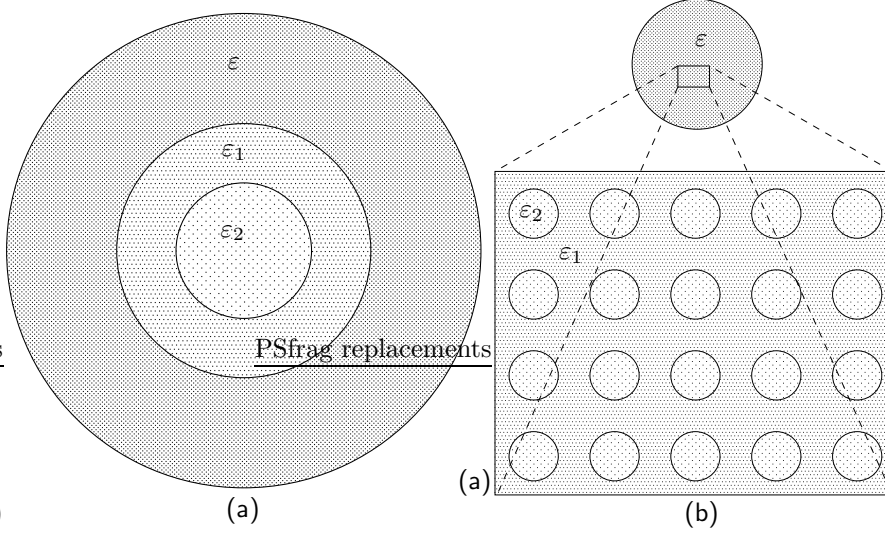


Figure 1. (a) EMA and (b) RAD approaches to dielectric mixtures.

τ^{-1} , there are only three material quantities that explicate electrical properties, ϵ , $\chi(0)$ and σ ,

$$\begin{aligned} \epsilon(\omega) &= \epsilon + \frac{\sigma}{i\epsilon_0\omega} & \text{for } \omega \gg \tau^{-1} \\ \varsigma(\omega) &= \sigma + i\epsilon_0\epsilon\omega \\ \epsilon(\omega) &= \epsilon + \chi(0) + \frac{\sigma}{i\epsilon_0\omega} & \text{for } \omega \ll \tau^{-1} \\ \varsigma(\omega) &= \sigma + i\epsilon_0[\epsilon + \chi(0)]\omega \end{aligned}$$

When the analytical solutions of binary mixtures in two-dimensions are considered, the EMA approach supposes two concentric dielectric disks with dielectric permittivities ϵ_1 and ϵ_2 such that they are embedded inside the effective medium with dielectric permittivity, ϵ , as presented in Fig. 1a. In the two-dimensional RAD approach, on the other hand, the composite medium is assumed to be composed of monodispersed inclusions (disks) at square lattice sides, as illustrated in Fig. 1b. The effective complex dielectric permittivities calculated by EMA [5, 6, 9] and RAD [10, 11], then, yield

$$\epsilon_{\text{EMA}} = \frac{\epsilon_2 \epsilon_1 + \epsilon_1^2 + \epsilon_2 \epsilon_1 q - \epsilon_1^2 q}{\epsilon_2 + \epsilon_1 - \epsilon_2 q + \epsilon_1 q} \quad (4)$$

$$\begin{aligned} \epsilon_{\text{RASS}} &= \epsilon_1 \frac{\pi - \pi\Lambda q + 4\Lambda^2 q(A + B)}{\pi + \pi\Lambda q + 4\Lambda^2 q(A + B)} \\ \Lambda &= \frac{\epsilon_1 - \epsilon_2}{\epsilon_1 + \epsilon_2} \end{aligned} \quad (5)$$

where, q is the concentration of the inclusion phases, which are denoted by subscript (2), ($0 \leq q \leq 1$). The parameters A and B are functions of the radius of the inclusion phase, $r \equiv \sqrt{q/\pi}$,

$$\begin{aligned}
 A = & 2r^3 \sum_{m=1}^{\infty} \frac{1}{r^4 - 16m^4} + \sum_{n=1}^{\infty} \sum_{m=1}^{\infty} \left[\frac{r - 2m}{(r - 2m)^2 - 4n^2} \right. \\
 & + \frac{r + 2m}{(r + 2m)^2 - 4n^2} + \frac{r - 2m + 1}{(r - 2m + 1)^2 - (2n - 1)^2} \\
 & \left. + \frac{r + 2m - 1}{(r + 2m - 1)^2 - (2n - 1)^2} \right] \quad (6)
 \end{aligned}$$

$$\begin{aligned}
 B = & 2r^3 \sum_{m=1}^{\infty} \frac{1}{r^4 - (2m - 1)^4} \\
 & + \sum_{n=1}^{\infty} \sum_{m=1}^{\infty} \left[\frac{r - 2m}{(r - 2m)^2 - (n - 1)^2} \right. \\
 & + \frac{r + 2m}{(r + 2m)^2 - (n - 1)^2} \frac{r - 2m + 1}{(r - 2m + 1)^2 - 4n^2} \\
 & \left. + \frac{r + 2m - 1}{(r + 2m - 1)^2 - 4n^2} \right] \quad (7)
 \end{aligned}$$

A and B values converge quickly a constant value for $n = m \geq 10$.

3. Numerical calculations

Analytical calculations of electromagnetic problems using Maxwell's equations, are limited to geometrical constraints. For some simple geometries with a small number of materials (regions) and symmetries, analytical solutions can be found [15, 16, 11, 17, 18]. The analytical solutions are obtained using methods of images [19, 20], orthogonal functions (Green functions) [21] and complex variable techniques (conformal mapping) [22, 20, 15]. The conformal mapping can only be applied to two-dimensional problems in which the third spatial axis is neglected. For more complex geometries and non-homogeneous regions composed of several materials, numerical solutions of partial differential equations and of integral equations have been developed [23] *e.g.*, the finite difference method, the finite element method, the method of moments and the boundary element method.

Numerical solutions of electrostatic problems within a non-conducting medium are based on solving Poisson's equation

$$\nabla \cdot (\epsilon \epsilon_0 \nabla \phi) = -\rho \quad (8)$$

where ϕ , and ρ denote the electrical potential and the total charge in the considered region, respectively. Moreover, if the medium is conductive where no free charges and

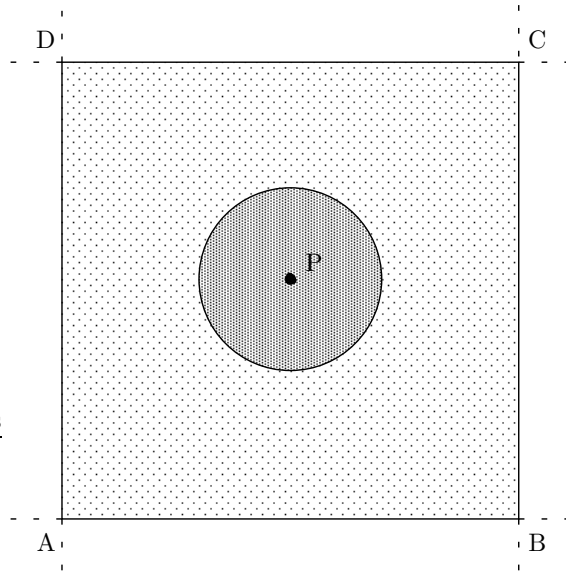


Figure 2. The unit cell of square lattice with corners at $ABCD$ used in the calculations. Dark region is the disk inclusion with ε_2 and σ_2 and the lighter region is the matrix media with ε_1 and σ_1 .

Table 1. Composite electric properties obtained from the analytical formulae.

Model	q	ε_M	ε_μ	σ/ε_0 [S/F]
EMA	0.1	2.28571429	2.42552966	0.13749080
RAD	0.1	2.28586956	2.42602610	0.13752067
EMA	0.2	2.61538462	2.95231624	0.16802403
RAD	0.2	2.61743641	2.95942150	0.16845390
EMA	0.3	3.00000000	3.62134985	0.20703632
RAD	0.3	3.01008959	3.66005320	0.20939659

sources of charges are allowed, then, the solution is given by

$$\nabla \cdot (\sigma \nabla \phi) = 0 \quad (9)$$

When the medium is a mixture of these two cases (lossy dielectric), it consists of dielectric and conductive components. The solution, then, becomes time dependent and is given by a complex electric potential in the region with the coupling of Eqs. (8) and (9), which is also known as the continuity equation.

$$\nabla \cdot (\sigma \nabla \phi) + \nabla \cdot \left[\frac{\partial}{\partial t} (\epsilon \epsilon_0 \nabla \phi) \right] = 0 \quad (10)$$

or equivalently in Fourier-space with frequency dependent properties,

$$\nabla \cdot \{ [\nu \epsilon_0 \varepsilon(\omega)] \nabla \phi \} = 0 \quad (11)$$

where no free charges are allowed in the region, due to conductivity of the medium (lossy dielectric). Note that $\varepsilon(\omega)$ in Eq. (11) is given in Eq. (1).

In this work, we have used a field calculation software, ‘ACE’, [24] based on the FEM. A square lattice unit-cell with a hard-disk inclusion was assumed, as shown in Fig. 2. The boundary conditions were chosen as follows; along line [AB] was the ground potential level, $V = 0$ V, along line [CD] it was 1 V, and the lines [AD] and [BC] were the symmetry lines (axes of reflection). The calculations were performed under steady-state periodic conditions. The region of interest is meshed using an triangular meshing technique in which we have limited number of triangles by ~ 8000 elements. The minimum triangle size was selected using the size of the considered inclusion geometry in the meshing procedure. Moreover, the quadratic shape function was used to solve in the FEM.

The complex permittivity of a heterogeneous medium can be calculated in several ways, *e.g.*, (i) by using the total current density, j , and the phase difference, θ [25, 26, 27, 28], (ii) Gauss’ law and losses [26, 29, 30] and lastly (iii) by using the average values of

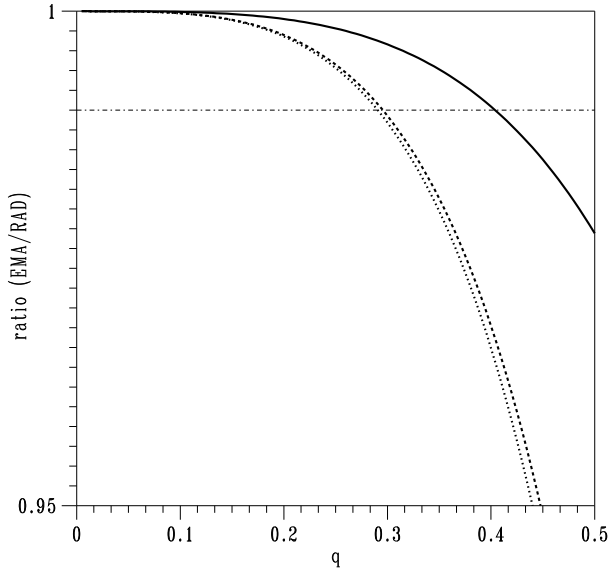


Figure 3. Comparison of the two analytical models. The solid (—), dashed (- - -) and dotted (·····) lines represent the ratios of the high frequency dielectric permittivity, ε_M , low frequency permittivity, ε_μ , and the conductivity, σ/ϵ_0 , values, respectively. The region above the thin chain (- · -) line marks the 1 %.

dielectric displacement $\langle \mathbf{D} \rangle$ and electric field $\langle \mathbf{E} \rangle$ [26, 31]. We have used the first two ways (i & ii) to calculate the complex dielectric permittivities, $\varepsilon(\omega)$ of the structures considered. The phase parameters, ε and σ , were frequency and voltage independent. The values of ε and σ are chosen such that the interfacial polarization observed has a relaxation time, τ , around 1 s. This is achieved when the matrix phase has $\varepsilon_1 \equiv \epsilon_1 = 2$ and $\sigma_1 = 1$ pS/m, and the inclusion phase has $\varepsilon_2 \equiv \epsilon_2 = 10$ and $\sigma_2 = 100$ pS/m. The normalized conductivity values, σ/ϵ_0 , are $\sigma_1/\epsilon_0 = 0.113$ S/F and $\sigma_2/\epsilon_0 = 11.3$ S/F, respectively. We have focused on two frequencies, $2\pi\mu\text{Hz}$ and $2\pi\text{MHz}$ which are, respectively, used as subscripts (μ) and (M) for the appropriate dielectric permittivity values. At these frequencies, the influence of interfacial polarization was negligible, $|\log \omega| \gg \tau^{-1}$, and the composite medium can be expressed with three parameters, ε_M , ε_μ [$\equiv \varepsilon_M + \chi(0)$] and σ/ϵ_0 .

4. Results and discussion

The concentration dependence of the electrical properties calculated using the analytical formulae of Eqs. (4) and (5) differ at some concentration level. This is illustrated in Fig. 3

by the ratio of resulting effective parameters. For concentration values higher than 30 % ($q > 0.3$), the effective medium quantities obtained from the two analytical approaches start to differ. The behavior of ratios for the dielectric permittivity at low frequencies, ε_{μ} and the conductivity, σ , were similar and the change with respect to concentration, q , was steeper compared to the ratio of the dielectric permittivity at low frequencies, ε_M . The difference between the models is due to the approximations and simplifications considered in the geometries. In RAD assumptions there are neighboring inclusions whose charge distributions (polarization) influence the polarization of the individual inclusions, however, in EMA the polarization of the inclusion is only due to the interface between the inclusion and the matrix phases. Accordingly, in the numerical simulations, three concentration levels were selected, $q = \{0.1, 0.2, 0.3\}$, and the ε_M -, ε_{μ} - and σ/ε_0 -values were calculated. The same quantities obtained from EMA and RAD are listed in Table 1 for comparison. The differences in the ε_M and σ/ε_0 values calculated from the analytical models are in the fourth, third and second number after the decimal point for $q = 0.1, 0.2, 0.3$, respectively. However, the change in ε_{μ} is larger for both models at the same concentrations.

In the simulations, we have assumed that the inclusion phase was a two-dimensional object, a *regular* polygon with n sides, as displayed in Fig. 4. The polygons were generated using a circle with radius, r , and a constraint on the area of the polygons, q . Then, the radius, r , as a function of n and q is expressed as,

$$r_n = \sqrt{\frac{q}{n \sin(\pi/n) \cos(\pi/n)}} \quad (12)$$

The denominator inside the square root approaches π as $n \rightarrow \infty$. The size of radius was also used for the meshing procedure of the computation domain where $r_n/15$ was the size of the minimum triangle. Furthermore, this approach leads to the finite-size scaling considerations [32, 33] in which as $n \rightarrow \infty$, the inclusion phase is a perfect disk. As mentioned previously, two different methods were used to calculate the electrical quantities of the binary mixture, and Table 2 presents the results. The first remark was that the difference between the obtained ε_{μ} -values using two different approaches. The discrepancy between ε_{μ}^a and ε_{μ}^b increased as the concentration level, q , was increased. Moreover, when the values were compared top those of Table 1, except ε_{μ}^b , the other calculated quantities had good agreement with the analytical models.

Obtained quantities, ε_M -, ε_{μ} - and σ/ε_0 , can be described by a trivial relation, which considers the finite-size behavior,

$$f(n, q) - \lambda \approx a_1(n - 2)^{\alpha_1(q)} + a_2(n - 2)^{\alpha_2(q)} \quad (13)$$

where $\lambda = f(\infty, q)$. We have also scaled the above equation with $n - 2$ since the calculations were performed in two-dimensions. The λ -values are presented in Table 2 as $n \rightarrow \infty$, except ε_{μ}^b all others were close to the data in Table 1. In Fig. 5, an example of the finite-size behavior is shown. A critical number of sides, n_c , is defined, such that over

TUNCER

Table 2. Electrical parameters calculated by the FEM.

n	ϵ_M^a	ϵ_μ^a	σ/ϵ_0^a [S/F]	ϵ_M^b	ϵ_μ^b	σ/ϵ_0^b [S/F]
$q = 0.1$						
3	2.31830984	2.55431772	0.14540117	2.31831000	2.57482200	0.14462477
4	2.29814032	2.46885006	0.14011433	2.29814046	2.48120081	0.13990578
5	2.29154397	2.44497599	0.13866220	2.29154405	2.45548560	0.13852250
6	2.28903383	2.43636313	0.13814092	2.28903405	2.44625458	0.13804715
7	2.28780142	2.43222046	0.13789067	2.28780167	2.44182314	0.13782876
8	2.28712945	2.43000429	0.13775702	2.28712965	2.43945636	0.13769620
9	2.28672438	2.42867095	0.13767662	2.28672448	2.43803276	0.13762992
10	2.28646432	2.42782513	0.13762567	2.28646448	2.43713033	0.13759796
11	2.28629434	2.42727218	0.13759236	2.28629442	2.43654060	0.13756319
12	2.28617467	2.42688644	0.13756913	2.28617471	2.43612935	0.13754747
14	2.28602947	2.42641794	0.13754093	2.28602973	2.43562974	0.13752268
16	2.28594550	2.42615013	0.13752482	2.28594567	2.43534447	0.13750994
18	2.28589649	2.42599233	0.13751533	2.28589650	2.43517637	0.13750239
99	2.28577330	2.42560592	0.13749210	2.28577345	2.43476492	0.13748560
∞	2.28576594	2.42558544	0.13749087	2.28576605	2.43474329	0.13747696
$q = 0.2$						
3	2.69416747	3.30221747	0.18974833	2.69416760	3.36013939	0.18911785
4	2.64801022	3.07703286	0.17563592	2.64801032	3.11023106	0.17541128
5	2.62892034	3.00133543	0.17099827	2.62892033	3.02810579	0.17088012
6	2.62304978	2.97945868	0.16966607	2.62304982	3.00451441	0.16958761
7	2.62025295	2.96934543	0.16905189	2.62025298	2.99363860	0.16899605
8	2.61869852	2.96379171	0.16871499	2.61869871	2.98767247	0.16866931
9	2.61776224	2.96046863	0.16851354	2.61776238	2.98410506	0.16847596
10	2.61716591	2.95837257	0.16838656	2.61716598	2.98185662	0.16836172
11	2.61677916	2.95701332	0.16830424	2.61677923	2.98039874	0.16827771
12	2.61650596	2.95606556	0.16824686	2.61650611	2.97938287	0.16822349
14	2.61616711	2.95488967	0.16817569	2.61616735	2.97812228	0.16815940
16	2.61598326	2.95424269	0.16813652	2.61598338	2.97742871	0.16812236
99	2.61560667	2.95293358	0.16805731	2.61560681	2.97602608	0.16806089
∞	2.61561521	2.95297927	0.16806011	2.61561540	2.97607565	0.16805491
$q = 0.3$						
3	3.15432863	4.44992747	0.25956453	3.15432877	4.59647254	0.25812644
4	3.07199643	3.93508366	0.22640982	3.07199661	4.00935583	0.22583378
5	3.02527912	3.72286805	0.21324951	3.02527918	3.77630766	0.21302790
6	3.01422774	3.67689028	0.21042426	3.01422781	3.72627694	0.21031765
7	3.00968689	3.65880191	0.20931774	3.00968704	3.70668244	0.20923851
8	3.00700955	3.64824288	0.20867221	3.00700972	3.69525097	0.20859681
9	3.00525073	3.64134674	0.20825088	3.00525070	3.68779013	0.20820236
10	3.00420698	3.63728448	0.20800287	3.00420720	3.68339788	0.20795785
11	3.00352151	3.63462285	0.20784042	3.00352166	3.68052130	0.20781141
12	3.00303949	3.63276735	0.20772723	3.00303968	3.67851699	0.20769857
14	3.00245464	3.63050408	0.20758916	3.00245485	3.67607184	0.20756988
16	3.00211061	3.62921448	0.20751059	3.00211061	3.67468077	0.20749301
99	3.00143716	3.62665177	0.20735438	3.00143741	3.67191430	0.20734844
∞	3.00147224	3.62677466	0.20736184	3.00147232	3.67204654	0.20735887

^a Calculated from the current and phase shift between the applied voltage and current.

^b Calculated using Gauss' law and the total losses in the medium.

Table 3. Finite-size behavior modeling parameters.

	q	$\log a_1^a$	α_1^a	$\log a_2^a$	α_2^a	$\log a_1^b$	α_1^b	$\log a_2^b$	α_2^b
ε_M	0.1	-1.500	-0.215	-4.174	-0.017	-1.500	-0.215	-4.172	-0.017
ε_μ	0.1	-0.930	-0.223	-3.530	-0.022	-0.895	-0.224	-3.487	-0.023
σ/ε_0	0.1	-2.145	-0.224	-5.077	-0.010	-2.178	-0.230	-5.014	-0.003
ε_M	0.2	-1.104	-0.220	-3.994	-0.015	-1.104	-0.220	-3.990	-0.015
ε_μ	0.2	-0.492	-0.230	-3.240	-0.022	-0.455	-0.231	-3.195	-0.022
σ/ε_0	0.2	-2.202	-0.230	-5.253	-0.008	-2.210	-0.233	-5.330	-0.005
ε_M	0.3	-0.806	-0.227	-3.724	-0.015	-0.806	-0.227	-3.722	-0.015
ε_μ	0.3	-0.127	-0.241	-2.970	-0.021	-0.083	-0.242	-2.926	-0.021
σ/ε_0	0.3	-1.829	-0.242	-4.951	-0.011	-1.840	-0.243	-4.993	-0.009

^a Obtained for values calculated by using the current and phase shift between the applied voltage and current.

^b Obtained for values calculated by using Gauss' law and the total losses in the medium.

this value, $n > n_c$, the effective properties of medium with regular polygons as inclusions are approximately similar to those of a medium with disk shape inclusions. The analysis showed that n_c is approximately 15 regardless the concentration levels considered, $q \leq 0.3$, and the error in the calculations is $< 0.01\%$ for $n_c > 15$, as displayed in Fig. 5. In fact, even an decagon ($n = 10$) can imitate a disk in which the error in the calculated electrical quantities is less than $< 0.1\%$. Furthermore, Eq. (13) is divided in two,

$$f(n, q) - \lambda \propto \begin{cases} (n-2)^{\alpha_1(q)} & n < 15 \\ (n-2)^{\alpha_2(q)} & n > 15 \end{cases} \quad (14)$$

In Table 3, the parameters of this behavior, Eq. (13), from a curve-fitting procedure are presented. All calculated quantities had similar behavior as in the Fig. 5. It was clear to us that the exponents were concentration independent, $\alpha \neq F(q)$. Moreover, although α_1 was constant for all considered quantities, α_2 was dependent on quantities. Finally, there was no trivial relation between concentration and obtained a values.

5. Conclusions

Calculations of effective electrical properties of binary dielectric mixtures were used to evaluate number of sides of a regular polygon in order the considered polygon to imitate a disk in computer calculations. We assumed a medium with inclusions as regular polygons with n sides, and calculated the electrical quantities, *i.e.*, dielectric permittivity and ohmic

conductivity by using the FEM, which were later compared to those of analytical formulae. In the simulations the concentration of the inclusion phase was constant and the shape of the inclusion was assumed to be regular polygons with n sides. The size of the polygon was used to control the FEM discretization of the computational domain. The analytical models were based on EMA and RAD, and two different procedures were used to estimate the effective properties. It was found that the procedure based on Gauss' law and the total losses in the medium was not that successful as the other one based on the current and phase shift between the applied voltage and current. In order to find the polygon to mimic a disk, the finite-size scaling behavior was introduced by considering the number of sides, n , in the regular polygons; in reality, a regular polygon with n sides becomes a disk as $n \rightarrow \infty$. It was found that for $n > 15$, there was no significant change in the effective electrical quantities of mixture for low concentrations, $q \leq 0.3$. Consequently, when the effective quantities of mixture with an regular decagon inclusion was compared with those obtained from the analytical formulae for a similar mixture with a disk inclusion, the percentage error between quantities yield less than 0.1 %.

Acknowledgments

Suggestions of Dr. Steven Boggs is acknowledged. Dr. Emre Tuncer is thanked for his fruitful comments.

References

- [1] E. Tuncer, Dielectric properties of composite structures and filled polymeric composite materials, Licenciate thesis–Tech. rep. 338 L, Department of Electric Power Eng., Chalmers University of Technology, Gothenburg, Sweden, 2000.
- [2] E. Tuncer, Dielectric relaxation in dielectric mixtures, PhD thesis, Chalmers University of Technology, Gothenburg, Sweden, 2001.
- [3] A. Priou, editor, *Progress in Electromagnetics Research*, Dielectric Properties of Heterogeneous Materials, Elsevier, New York, 1992.
- [4] A. Sihvola, *Electromagnetic mixing formulas and applications*, volume 47 of *IEE Electromagnetic Waves Series*, The Institute of Electrical Engineers, London, 1999.
- [5] J. C. M. Garnett, *Philosophical Transactions of Royal Society of London A* **203**, (1904), 385.
- [6] O. Wiener, *Der Abhandlungen der Mathematisch-Physischen Klasse der Königl. Sächsischen Gesellschaft der Wissenschaften* **32**, (1912), 509.
- [7] K. W. Wagner, *Archiv für Electrotechnik* **II**, (1914), 371.
- [8] R. Sillars, *Journal of Institution of Electrical Engineers* **80**, (1937), 378.

- [9] P. A. M. Steeman and F. H. J. Maurer, *Colloid & Polymer Science* **268**, (1990), 315.
- [10] L. Rayleigh, *Philosophical Magazine* **34**, (1892), 481.
- [11] Y. P. Emets, *Journal of Experimental and Theoretical Physics* **87**, (1998), 612.
- [12] A. Franklin, *Physics in Perspective* **1**, (1999), 35.
- [13] A. K. Jonscher, *Dielectric Relaxation in Solids*, London: Chelsea Dielectric, London, 1983.
- [14] P. Debye, *Polar Molecules*, Dover Publications, New York, 1945.
- [15] E. Weber, *Electromagnetic Theory: Static Fields and Their Mappings*, Dover Publications Inc., New York, 1965.
- [16] Y. Emets and Y. P. Onofrichuk, *IEEE Transactions on Dielectrics and Electrical Insulation* **3**, 87 (1996).
- [17] J. D. Jackson, *Classical Electrodynamics*, John Wiley & Sons, Inc., Toronto, Canada, second edition, 1975.
- [18] C. J. F. Böttcher, *Theory of Electric Polarisation*, Elsevier Publishing Company, Amsterdam, 1952.
- [19] R. S. Elliot, *Electromagnetics*, McGraw-Hill Book Company, New York, 1966.
- [20] L. Eyges, *The Classical Electromagnetic Field*, Dover, New York, 1972.
- [21] K.-H. Steiner, *Interactions between Electromagnetic Fields and Matter*, volume 1 of *Vieweg Tracts in Pure and Applied Physics*, Pergamon Press, Oxford, 1973.
- [22] S. Ramo, J. R. Whinnery, and T. van Duzer, *Fields and Waves in Communication Electronics*, Wiley, New York, third edition, 1994.
- [23] J. R. C. Richard, *Computational Methods for Electromagnetics and Microwaves*, John Wiley & Sons, Inc., New York, 1992.
- [24] Asea Brown Boveri Corporate Research, Västerås Sweden, *Ace 2.2 Users Manual and Ace Command Language Reference*, 1993.
- [25] A. von Hippel, editor, *Dielectric Materials and Applications*, The Technology Press of M.I.T.-WILEY, Boston, 1954.
- [26] B. K. P. Scaife, *Principles of Dielectrics*, Oxford Science Publications, 1998.
- [27] E. Tuncer, S. M. Gubański, and B. Nettelblad, *Journal of Applied Physics* **89**, (2001), 8092.

- [28] E. Tuncer, B. Nettelblad and S. M. Gubański, Non-debye dielectric relaxation in binary dielectric mixtures (50-50):randomness and regularity in mixture topology, *Journal of Applied Physics* **XX**, (2002), XXXX.
- [29] B. Sareni, L. Krähenbühl, and A. Beroual, *Journal of Applied Physics* **80**, (1996), 4560.
- [30] E. Tuncer and S. M. Gubański, Dielectric properties of different composite structures, in *Dielectric and Related Phenomena DRP'98: Polymers and Liquid Crystals*, edited by A. Wlochowicz and E. Targosz-Wrona, volume 4017 of *Proceedings of SPIE*, pages 136–142, Washington, 1998, Technical University of Lodz, Branch in Bielsko-Biala, Poland, SPIE, The International Society for Optical Engineering.
- [31] L. Landau and E. Lifshitz, *Electrodynamics of continuous media*, volume 8 of *Course of Theoretical Physics*, Pergamon Press, New York, 2nd edition, 1982.
- [32] M. Plischke and B. Bergersen, *Equilibrium Statistical Physics*, World Scientific, London, second edition, 1994.
- [33] J. L. Cardy, editor, *Finite-Size Scaling*, Current Physics – Sources and Comments, North-Holland, Amsterdam, 1988.

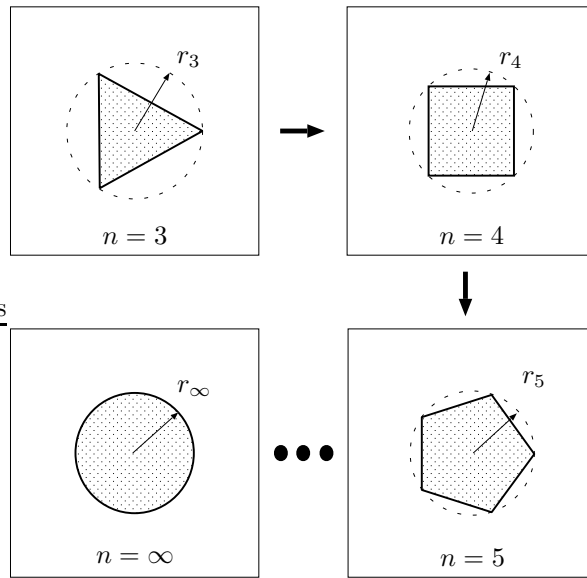


Figure 4. Finite-size scaling of the inclusion shapes (polygons).

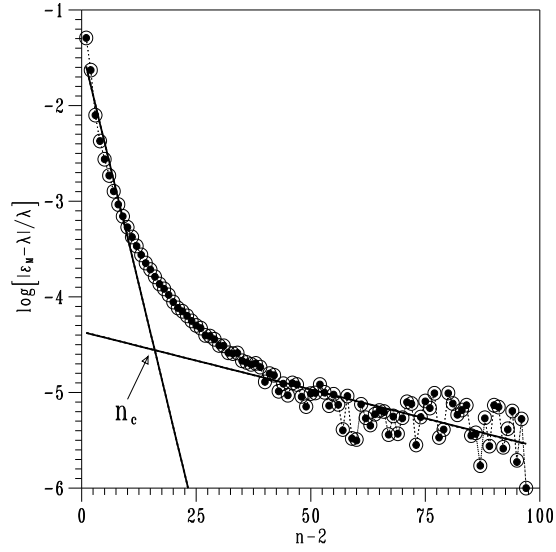


Figure 5. Normalized dependence of incremental high frequency dielectric permittivity, $|\epsilon_M - \lambda|/\lambda$ on number of regular polygon sides, n . The symbols open (○) and filled (●) indicate the solutions obtained using the current density and phase shift between the applied voltage and current and using Gauss' law and the total losses in the medium, respectively. The solid lines (—) represents the fitted curves. n_c is the critical side number for regular polygons.